XX. APPLIED PLASMA RESEARCH[*]

A. Active Plasma Systems

Academic and Research Staff

Prof. L. D. Smullin   Prof. R. R. Parker
Prof. R. J. Briggs   Prof. K. I. Thomassen

Graduate Students

D. S. Guttman   B. R. Kusse   J. A. Mangano
F. Herba   R. K. Linford J. A. Rome

RESEARCH OBJECTIVES

The interests of the Active Plasma Systems Group cover a variety of topics in gaseous plasmas and charged-particle beams, the majority of which have as central focus the generation of highly ionized plasmas for application to controlled fusion. In the realm of "turbulent plasma" studies, we shall continue our work on the beam-plasma discharge with present emphasis on techniques for describing and measuring a turbulent plasma, possible plasma sources other than gas injection, and ion heating by excitation at the ion-cyclotron frequency. Related topics are the heating of plasmas by stochastic fields and the synthesis by injection of electron and ion beams in vacuum. A discussion of particular topics follows.

1. Radiation and Turbulence in Beam-Plasma Discharge

The radiated RF spectrum of the BPD is complex and shows marked incoherencies, both temporal and spatial. Besides the primary interaction at the upper frequency, there is a very broad noiselike spectrum in the range (typically) 100 MHz-2000 MHz. We plan to study the spatial coherence (correlation) of this noise and will relate it to fluctuations in the plasma density. There are some basic problems in relating the radiated field from a plasma of finite dimensions to its internal structure, and it is not yet clear how far one-dimensional theory can be pushed.

L. D. Smullin, R. R. Parker

2. Ion-Cyclotron Heating

We plan to exploit the possibility of heating a plasma by using a short-wavelength coil coupled to a plasma column in a nonuniform (mirror) magnetic field. Our initial experiments have shown that it is possible, in this way, to transfer energy to the plasma over a broad range of frequencies, corresponding to local ion-cyclotron resonance under different parts of the coil. It would appear that this should lead to more uniform heating than has been the case in previous experiments, thereby producing a hot plasma that would be less susceptible to velocity-space instabilities.

R. R. Parker

3. Electric Arc Thruster Study

An electric thruster using teflon as a fuel element is now used in a Lincoln Laboratory, M. I. T., communication satellite. An arc discharge over the teflon surface is repelled by the return current, thereby forming a type of rail accelerator. Gasdynamic thrust also plays a role.

The purpose of this research program is to study the discharge properties and develop a model to explain the observed thrust (several pounds during the 1-μsec discharge).

K. I. Thomassen

4. Plasma Stabilization by Feedback

Several recent experiments on the Ogra machine, in U. S. S. R., have demonstrated the stabilization of flutes and cyclotron waves by feeding back the low-frequency oscillations from a Langmuir probe to conducting plates running the length of the discharge. The method is similar to that used by Melcher to stabilize a Rayleigh-Taylor instability.

In our experiment we shall use a hot-cathode PIG discharge, which is known to be unstable to resistive drift waves, to explore the mechanisms for stabilizing the discharge.

K. I. Thomassen, R. R. Parker

5. Titanium Hydride Plasma Source

A commercially available hydrogen-loaded titanium cylinder, with an insulating gap on its surface, expels plasma when an arc is struck across the gap. This source is being explored to determine its suitability as a highly ionized plasma source.

K. I. Thomassen

6. Stability of Sheared Electron Flow

In high-perveance magnetically focused electron beams, a substantial velocity shear can be generated by the potential depression in a drift region. We are, at present, investigating the stability of oscillations in such systems; part of the practical motivation is a better understanding of noise generation or amplification in high-power beam tubes. We have derived general criteria for stability, and we are now investigating in detail the stability properties of particular velocity profiles.

R. J. Briggs

7. Plasma Synthesis

As a variation on our beam-plasma discharge studies, we are investigating the generation of a plasma in a "hard" vacuum by the injection of counterflowing electron and ion beams. The ion source is a solid thermionic emitter which is capable of 1-5 mA emission of potassium ions. The system has been constructed and the ion emitters tested; preliminary tests of the injection of both ions and electrons are under way.

The basic goal of this research is to test in a small-scale experiment the feasibility of plasma accumulation and heating by the nonadiabatic effects arising from cooperative

instabilities in a two-stream configuration.

<div align="right">R. J. Briggs</div>

8. Waves in Inhomogeneous Media

During the past year, we developed a technique for determining the critical lengths for absolute instabilities in mildly inhomogeneous media. We intend to investigate further the connections between the stability of infinite homogeneous media and mildly inhomogeneous systems.

<div align="right">R. J. Briggs</div>

1. ION-CYCLOTRON RESONANCE IN A NONUNIFORM MAGNETIC FIELD

Work has begun on investigating the possibility of using a short-wavelength coil to transfer power to a plasma in a nonuniform magnetic field. The basic idea is to excite the coil at a frequency that will be equal to the ion-cyclotron frequency somewhere under the coil. In this way, relatively broadband coupling could be achieved, and the possibility would then exist of using a wideband noise source for heating. This in turn should result in uniform heating of the plasma.

The initial experiment of measuring the resistance of a short-wavelength coil surrounding a plasma in a mirror field has been carried out. The theoretical and experimental results are discussed in this report.

Theoretical Discussion

We consider the system shown in Fig. XX-1, which consists of a plasma column surrounded by a reverse-turn coil. The plasma is assumed to be in a magnetic field that may be nonuniform. We also assume that the plasma is cold, and its electrical properties may be characterized by the cold-plasma dielectric tensor.

If an RF source with current I is connected to the terminals of the coil, the power delivered by the source will be $\frac{1}{2} R |I|^2$, where R is the real part of the impedance of the coil. By applying Poynting's theorem to the cylinder whose cross section is shown
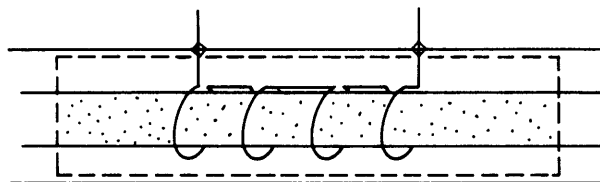

Fig. XX-1. Reverse-turn RF coil coupled to a plasma column.

dashed in Fig. XX-1, and neglecting wave generation in the axial direction, we find for the resistance

$$R = \frac{\omega \epsilon_o}{|I|^2} \, \text{Im} \int \bar{E}^* \cdot \bar{\bar{K}} \cdot \bar{E} \, d\bar{r}, \tag{1}$$

where the volume integral is carried out over the volume enclosed by the cylinder. (We have assumed perfectly conducting walls and that the coil itself has zero resistance.)

To make further use of Eq. 1, we need to find $\bar{\bar{E}}$, and this requires the self-consistent solution of Maxwell's equations. For the case of uniform magnetic field, this problem has been solved by Stix[1] who simplified the problem by neglecting electron inertia. By examining the solution given by Stix, it is possible to show that, under certain conditions, the expression given in Eq. 1 for the resistance will be accurate even if the vacuum electric field is used, rather than the self-consistent electric field. The conditions for this are $\beta^2 \gg k_o^2 K_\perp$ and $\beta a \lesssim 1$, where β is the dominant wave number associated with the coil, $k_o = \frac{\omega}{c}$, $K_\perp$ is the diagonal component of the dielectric tensor, and a is the radius of the plasma column. These conditions ensure that the coil does not couple strongly to any of the normal modes of the plasma column.

These conclusions were realized some time ago by Glenn,[2] who also realized the importance of using a coil of finite wavelength. The finite wavelength of the coil is necessary in order to periodically reverse the sign of the polarization charge which results, because of ion motion. The axial variation of the polarization charge drives axial electron currents that maintain charge neutrality, thereby allowing the vacuum field to penetrate. Neutralization cannot occur for a coil of zero wavelength, that is, a long solenoid, and for this case Eq. 1 is not correct to any nontrivial order if the vacuum field is used.

Based on these results for the case of the uniform magnetic field, we propose to use Eq. 1 with the vacuum electric field for the case of the nonuniform magnetic field. In order that the required charge neutrality can be maintained, however, we assume that the magnetic field is symmetric with respect to the midplane of the coil.

For a coil whose radius is less than its axial wavelength, the electric field is essentially proportional to radius. If the current in the coil is I, and the wavelength is λ, the fundamental component of the electric field is

$$\bar{E}_o = \hat{i}_\theta \frac{j 2 \omega \mu_o r I}{\lambda} \sin \frac{2\pi}{\lambda} z, \tag{2}$$

where z is the axial coordinate, and z = 0 is located at the center of the coil. Equation 2 is valid under the coil, while near the ends of the coil the field rapidly decays to zero. While Eq. 2 is not strictly valid near the ends, we shall neglect end effects, and assume that $\bar{E}_o$ is given by Eq. 2 for $|z| < L/2$, where L is the length of the coil, and

zero for $|z| > L/2$. We shall also neglect the contribution of other space harmonics. Inserting Eq. 2 into Eq. 1, we obtain

$$R = \frac{4\omega^3 \mu_o^2 \epsilon_o}{\lambda^2} \, \text{Im} \int \frac{\omega_p^2(\bar{r})}{\omega_c^2(\bar{r}) - \omega^2} \, r^2 \sin^2 \frac{2\pi}{\lambda} z \, d\bar{r} \tag{3a}$$

$$= 2\pi \frac{\omega^3 \mu_o^2 \epsilon_o \omega_p^2 a^4}{\lambda^2} \, \text{Im} \int_{-L/2}^{L/2} \frac{\sin^2 \frac{2\pi}{\lambda} z}{\omega_c^2(z) - \omega^2} \, dz. \tag{3b}$$

Here ω_p and ω_c are the ion plasma and cyclotron frequencies, respectively. In obtaining Eq. 3b from Eq. 3a, we have neglected the spatial variation of the density caused by the bulging of the magnetic field lines.

The integral in Eq. 3b, apart from the $\sin^2 \frac{2\pi}{\lambda} z$ factor, is similar to that defining the resistance of a planar capacitor filled with nonuniform, cold plasma.[3] As in the last case, the integral is improper, since it involves integration through a pole. This is resolved by giving the frequency a small, negative, imaginary part and then analytically continuing to the Im $\omega = 0$ axis. The result is

$$R(\omega) = \sum_i 2\pi^2 \frac{\omega^3 \mu_o^2 \epsilon_o \omega_p^2 a^4}{\lambda^2} \frac{\sin^2 \frac{2\pi}{\lambda} z_i}{\omega_c(z_i) |\omega_c'(z_i)|}, \tag{4}$$

where z_i are the roots of the equation $\omega_c^2(z_i) = \omega^2$; $|z_i| < \frac{L}{2}$.

An interpretation of Eq. 4 can be made with the aid of Fig. XX-2. In Fig. XX-2a, we show a sketch of the cyclotron frequency as a function of z, and indicate the positions where local resonance is occurring, that is, where $\omega_c = \omega$. Since the electric field is varying sinusoidally, as in Fig. XX-2b, the electric field at the position of resonance will in general be nonzero, and hence the current density will be infinite. But since the current density is infinite over zero width, the total power absorbed, and hence the resistance, are finite, thereby giving rise to the result in Eq. 4.

It is of interest to see how a nonzero collision frequency modifies this result. For this purpose, we take the cyclotron frequency to be of the form

$$\omega_c^2 = \omega_{co}^2 \left(1 + \left(\frac{z}{\ell} \right)^2 \right),$$

where ω_{co} and ℓ are constant, and insert a phenomenological collision frequency, ν, into the dielectric tensor. This can be accomplished readily by replacing the ion mass, m_i, by $m_i \left(1 - j \frac{\nu}{\omega} \right)$. The result can then be integrated and expressed in
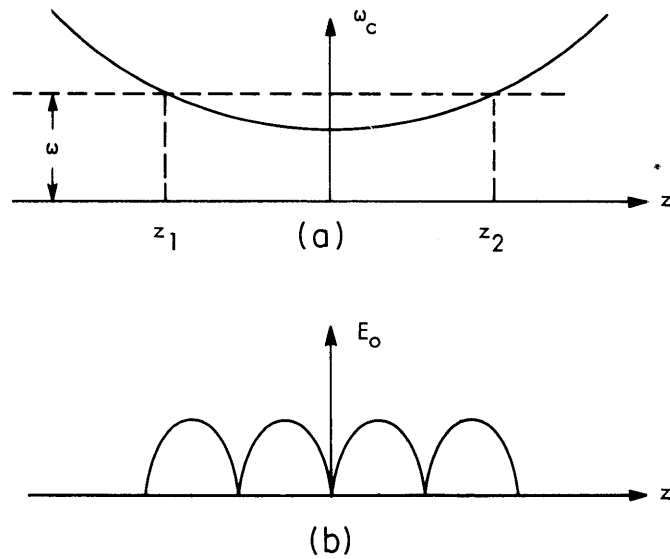
Fig. XX-2. (a) Shape of the magnetic field, showing positions of local resonance. (b) Axial variation of the magnitude of the electric field.

terms of the sine and cosine integral of complex argument. We find for the resistance R,

$$
R = \pi \frac{\omega^3 \epsilon_0 \mu_0^2 a^4 \omega_p^2 \ell}{\lambda^2 \omega_{co}^2} \operatorname{Im} \left\{ \frac{1 - \cos \frac{4\pi\ell}{\lambda} a}{a} \left[\ln \left(a - \frac{L}{2\ell} \right) - \ln \left(a + \frac{L}{2\ell} \right) \right] \right.
$$

$$
- \cos \frac{4\pi\ell}{\lambda} a \left[\operatorname{Cin} \left(\frac{4\pi\ell}{\lambda} \left(a + \frac{L}{2\ell} \right) \right) - \operatorname{Cin} \left(\frac{4\pi\ell}{\lambda} \left(a - \frac{L}{2\ell} \right) \right) \right]
$$

$$
\left. + \sin \frac{4\pi\ell}{\lambda} a \left[\operatorname{Si} \left(\frac{4\pi\ell}{\lambda} \left(a + \frac{L}{2\ell} \right) \right) - \operatorname{Si} \left(\frac{4\pi\ell}{\lambda} \left(a - \frac{L}{2\ell} \right) \right) \right] \right\}, \tag{5}
$$

where $a = (\Omega^2 - 1 + jN\Omega)^{1/2}$, $\Omega = \dfrac{\omega}{\omega_{co}}$ and $N = \dfrac{\nu}{\omega_{co}}$. The functions Cin and Si are defined in Abramowitz and Stegun.[4]

For a pure real or pure imaginary, that is, for $\nu = 0$, Eq. 5 reduces to Eq. 4. For small, but nonzero ν, the precise effect is hard to estimate. It is possible, however, to show that for $N^{1/2} \gtrsim \dfrac{\lambda}{\ell}$, the effect will be to smear out $R(\omega)$ as given in Eq. 4 near those frequencies for which $\sin^2 \dfrac{2\pi}{\lambda} z_i = 0$.

Experiment

To test our theory, a two-wavelength coil was inserted into System D, the beam-plasma discharge located at the Francis Bitter National Magnet Laboratory. It was
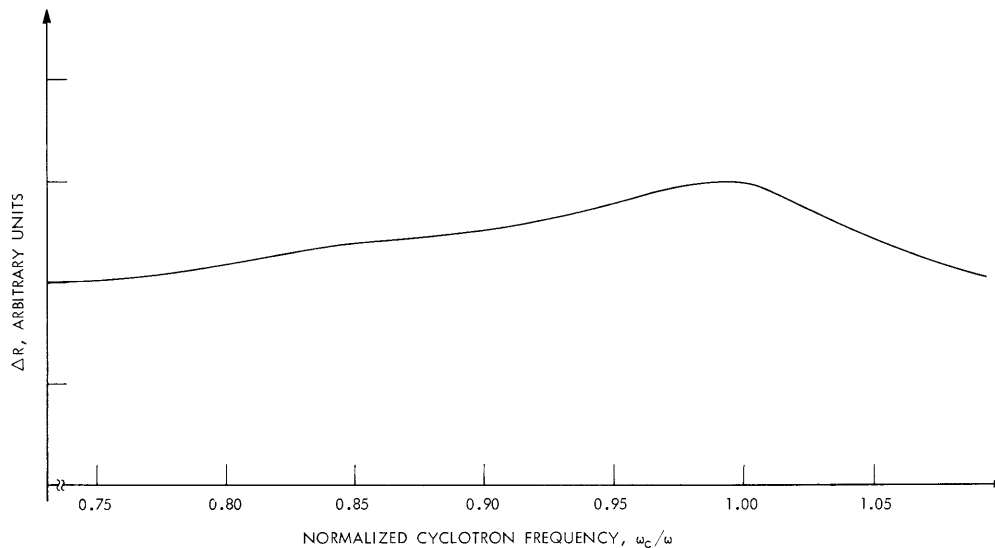
Fig. XX-3. Measured change in the resistance of the coil vs normalized cyclotron frequency.

found to be much easier to measure the resistance of the coil as a function of ω_c, rather than of ω. Hence the experiment consisted of recording the coil resistance of a fixed frequency, ω, as the magnetic field was swept.

The result of a typical experimental run is shown in Fig. XX-3, where we have plotted ΔR, the difference between coil resistance with and without a plasma, against ω_c/ω. While Eq. 4 appears to explain the main features of the curve, there are two discrepancies between the experimental results and the theory. First, the experiment reveals a background resistance whose magnitude is approximately twice that of the "resonant" part of the resistance; and second, only one relative peak in the resistance curve has been definitely identified, rather than the two peaks predicted by Eq. 4. It is possible that one effect of nonzero collision frequency as given in Eq. 5 is to smear out the other distinct resonance. Numerical evaluation of Eq. 5 will be carried out to see if this might be the case.

R. R. Parker

References

1. T. H. Stix, The Theory of Plasma Waves (McGraw-Hill Book Company, Inc., New York, 1962).

2. W. Glenn, "Plasma Diagnostics near Ion-Cyclotron Resonance," Ph.D. Thesis, Massachusetts Institute of Technology, 1966.

3. H. M. Schneider, "Oscillations of an Inhomogeneous Plasma Slab," Ph.D. Thesis, Massachusetts Institute of Technology, 1968.

4. M. Abramowitz and I. A. Stegun, Handbook of Mathematical Functions (Dover Publications, New York, 1965).

XX. APPLIED PLASMA RESEARCH*

B. Plasma Effects in Solids

Academic Research Staff

Prof. G. Bekefi
Prof. G. A. Baraff

Graduate Students

S. R. J. Brueck   C. S. Hartmann   D. A. Platts
E. V. George   R. N. Wallace

RESEARCH OBJECTIVES

We are continuing our studies of many-body, plasmalike effects of free carriers in solids. We emphasize those aspects of the problem that have to do with unstable modes of oscillation and wave propagation when the solid is subjected to external electric and/or magnetic fields. At the present time, we are concentrating our efforts on the microwave emission from Indium Antimonide at 77°K and on the microwave and radio emission that we have recently discovered in Bismuth Antimony alloys at 4°K. These emissions are still largely not understood. Before a theoretical model can be constructed two major experimental questions need to be answered. (i) What are the dispersion characteristics of the unstable waves? (ii) To what extent do contacts play a role in generating or triggering the instability? Partial answers to these questions have been obtained during the past year.

G. Bekefi

1. MICROWAVE INSTABILITIES IN A SEMICONDUCTOR SUBJECTED TO DC ELECTRIC AND MAGNETIC FIELDS

Phonon Effects

Many authors have theorized that the responsible mechanism for the generation of low-field microwave noise was the interaction of phonons with drifting electrons. If phonons are the major generating mechanism for the microwave emission and if they propagate at some angle to the magnetic field, then when these phonons strike the surface of the sample they should perturb the surface in some manner. If this hypothesis is correct, it may be possible to detect this surface motion, and, from its frequency spectrum and its dependence on the electric and magnetic field applied to the sample, to verify the existence of phonons that behave in a manner similar to the observed microwave emission. Moreover, since the conversion of phonon waves to electromagnetic waves is very weak, one should also be able to verify that the phonons are the primary generating species for the radiation or that they are only secondary (i.e., being

---

themselves generated by the microwave radiation) generating species.

It is necessary, therefore, to estimate (with order-of-magnitude calculations) the maximum motion of the surface. If the radiation possesses some amount of phase coherence (recent experiments with the spiked emission seem to indicate this), then we can write[1]

$$\langle P \rangle_{E.M.} = \gamma \langle P \rangle_{Acoustic},$$

where

$\langle P \rangle_{E.M.}$ = average electromagnetic power emitted at frequency ν

$\langle P \rangle_{Acoustic}$ = average acoustic power at frequency ν

γ = conversion efficiency.

Now,[1]

$$\langle P \rangle_{Acoustic} \approx A \frac{4\pi^2 \nu^2}{v_{sound}} Cu^2,$$

where

ν = frequency

v_s = sound velocity

C = elastic constant

A = surface area of the sample

u = displacement.

Using characteristic values of these constants for InSb, we obtain

$$\langle P \rangle_{Acoustic} \approx 10^4 \nu^2 u^2.$$

For an emitted power (at ~100 MHz) of ~10^{-6} W, we obtain

$$u \approx \frac{1}{\sqrt{\gamma}} 10^{-3} \overset{\circ}{A}.$$

The value of γ is of order –60 dB to –70 dB.[1] This means that

$$u \approx 1 \text{ \AA}$$

if phonons are the generating mechanism for the radiation. We shall illustrate a method for making very small displacement measurements.

Phase Modulation in a Michelson Interferometer

In this analysis we shall neglect the radial dependence of the electric field of the laser beam; that is,

$$E_{laser} = E \ e^{-(r/r_o)^2} \ e^{j(\omega t - kz)}$$

$$\approx E_o \ e^{j(\omega t - kz)}.$$

The radial dependence can be included in the analysis if one wishes, the only difference will be that in the final result an integration over r (also an integration over ϕ if the laser is not in the TEM_{00n} mode) will be required. It is also necessary that $2\left|(Z_1 - Z_2)\right| <$ coherence length of the laser. This is easily achieved if the laser operates in a single transverse and longitudinal mode. The laser used in this experiment operated in a single transverse mode, but ran in a multilongitudinal mode. (See Fig. XX-4.)

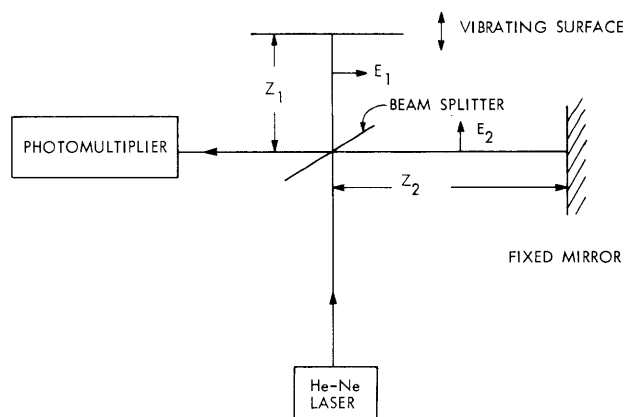We assume that the displacement of the vibrating surface, over the spot size of the

Fig. XX-4. Modified Michelson interferometer.
Z_1 = Distance from the beam splitter to the equilibrium position of the vibrating surface.
Z_2 = Distance from the beam splitter to the fixed mirror.
E_1, E_2 = Electric field of the laser beam in the respective arms of the interferometer.

laser beam at the surface, is given by

$$S = S_o \sin \omega_m t,$$

where S_o is the amplitude of vibration, and ω_m is the driving frequency. We shall neglect the Doppler-shifted frequency resulting from surface velocity and its resultant spectrum.

The output current of the photomultiplier will be of the form

$$i(t) = K \left| (E_1 + E_2)(E_1 + E_2)^* \right|, \tag{1}$$

where K is a proportionality constant depending on the characteristics of the photomultiplier. Now (note the beam splitter transmission coefficient is contained in E_{01} and E_{02}),

$$E_1 = E_{01} \exp\left[j \left(\omega_c t + \left(\frac{4\pi}{\lambda_c} \right) Z_1 + \left(\frac{4\pi}{\lambda_c} \right) S \right) \right]$$

and

$$E_2 = E_{02} \exp\left[j \left(\omega_c t + \frac{4\pi}{\lambda_c} Z_2 \right) \right],$$

where $f_c = \dfrac{\omega_c}{2\pi}$, λ_c are the frequency and wavelength of the He-Ne laser beam ($\lambda_c = 6328 \,\overset{\circ}{A}$). Substituting these values in Eq. 1 and collecting terms, we obtain

$$i(t) = K \left\{ E_{01}^2 + E_{02}^2 + 2 E_{01} E_{02} \cos \left(\eta - \xi + \delta \sin \omega_m t \right) \right\}, \tag{2}$$

where

$$\eta = \left(\frac{4\pi}{\lambda_c} \right) Z_1 \ ; \ \xi = \frac{4\pi}{\lambda_c} Z_2$$

and

$$\delta = \frac{4\pi}{\lambda_c} S_o.$$

If the interferometer were optically stable, with regard to mirror vibrations, then $\eta - \xi$ could be replaced by some constant θ; that is,

$$\eta - \xi = \theta \quad \text{(optically stable)}.$$

The problem is more complex if the interferometer is not optically stable, since in general random vibrations in, say, η are not correlated with vibrations in ξ. In this

case $\eta - \xi$ cannot be replaced by θ.

Considering the optically stable case and making use of the Bessel expansions,

$$\cos (\delta \sin \omega_m t) = J_0(\delta) + 2 \sum_{n=1}^{\infty} J_{2n}(\delta) \cos 2n\omega_m t$$

$$\sin (\delta \sin \omega_m t) = 2 \sum_{n=1}^{\infty} J_{2n-1}(\delta) \sin (2n-1)\omega_m t,$$

we obtain

$$i(t) = K \left\{ E_{01}^2 + E_{02}^2 + 2E_{01}E_{02} \left\{ J_0(\delta) + 2 \sum_{n=1}^{\infty} J_{2n}(\delta) \cos 2n\omega_m t \right\} \cos \theta \right.$$

$$\left. - 4E_{01}E_{02} \left\{ \sum_{n=1}^{\infty} J_{2n-1}(\delta) \sin (2n-1)\omega_m t \right\} \sin \theta \right\}. \tag{3}$$

The frequency spectrum consists of a DC term, the modulation frequency, and its harmonics. Notice that the amplitude of, say, $n\omega_m$ is given only by $J_n(\delta)$. This spectrum and the form of δ, that is, $\delta = \frac{4\pi}{\lambda_c} S_o$, independent of ω_m, is a form of phase modulation.

In order to verify the theory, a small mirror was mounted on a ceramic transducer.
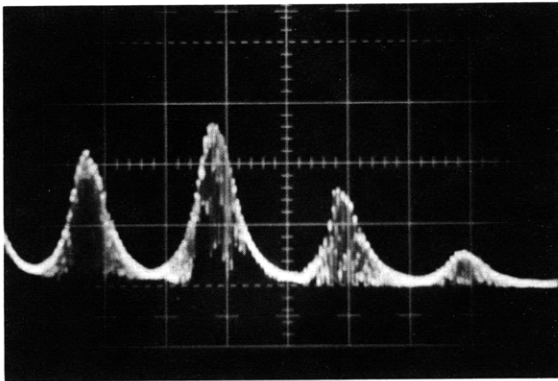

Fig. XX-5.
Spectrum analyzer output for an arbitrary value of S_o. Horizontal scale (frequency) 1 kHz/cm center frequency = 5 kHz. Vertical scale is power output in arbibtary units.

Any desirable value of S_o could be obtained by adjusting the driving voltage to the ceramic transducer. The output of the photomultiplier was fed into a spectrum analyzer. Figure XX-5 illustrates the output of the spectrum analyzer for some arbitrary value of S_o. It was possible experimentally to obtain the first few zeros of $J_n(\delta)$ by adjusting S_o.

Table **XX**-1.   Zeros of $J_m(\delta)$ for several modulation frequencies.

Modulation Frequency (Hz)	First Zeros						Second Zeros			
	$J_1(\delta) = 0$ $\delta = 3.882$		$J_2(\delta) = 0$ $\delta = 5.135$		$J_3(\delta) = 0$ $\delta = 6.379$		$J_1(\delta) = 0$ $\delta = 7.016$		$J_2(\delta) = 0$ $\delta = 8.417$	
	Volts	Normalized	Volts	Calculated	Volts	Calculated	Volts	Calculated	Volts	Calculated
1000	93	3.88	124	5.18	157	6.56	175	7.31	200	8.35
2000	76	3.88	104	5.32	126	6.45	134	6.85	164	8.39
3000	83	3.88	118	5.52	142	6.65	154	7.21	186	8.70
4000	72	3.88	92	4.97	—	—	130	7.02	151	8.14

By changing the modulating frequency, we could verify the form of δ. That is, δ should be independent of ω_m, within the frequency sensitivity of the transducer, whereas, if the spectrum were a form of frequency modulation, δ would vary inversely with ω_M. Table XX-1 lists the values of some of the zeros of $J_n(\delta)$ for several modulation frequencies. Although Eq. 3 predicts that by suitable adjustment of θ either the odd or even frequency harmonics can be made to vanish, this was not possible experimentally, because of small vibrations in the mirrors of the interferometer.

As we have pointed out, the amplitudes of vibration which we seek are small, consequently δ is small. Keeping only the lowest order term in Eq. 3, we have

$$i(t) \cong K\left[E_{01}^2 + E_{02}^2 + 2E_{01}E_{02}\left\{\cos\theta - 2\delta(\sin\omega_{mt})\sin\theta\right\}\right]. \tag{4}$$

To obtain a value for the minimum detectable surface motion, the ceramic transducer was replaced by a quartz single-crystal transducer. The thickness of the transducer was chosen so that its first resonant frequency occurred at approximately 30 MHz. For this crystal,

$$S_{o_{DC}} = d_{\parallel}V = 2 \times 10^{-10} \, V,$$

where

$$S_{o_{DC}} = \text{displacement off resonance (in cm)}$$

$$V = \text{voltage applied to the crystal (in Volts)}$$

On resonance, to a fair approximation, one can write

$$S_{o_{Resonance}} \approx QS_{o_{DC}},$$

where Q is the Q of the quartz transducer.

Table XX-2. Sensitivity of quartz transducer.

Frequency	Minimum Detectable RF Voltage (peak-to-peak) (V)	Minimum Detectable Motion (Å)
115 kHz	2	0.04
520 kHz	0.5	0.01
29.4 MHz	0.056	0.4 (Q≈300)

As before, the output of the photomultiplier was fed into a spectrum analyzer and the minimum detectable signal above receiver noise was recorded. Table XX-2 lists the results of this experiment.

Experimental Results

In order to obtain some amount of optical stability, the sample of InSb was mounted firmly to a cold finger. Figure XX-6 illustrates this new holder. The surface of the InSb crystal was mirror polished and a lens was incorporated into one arm of the Michelson cavity. A probe was also mounted close to the sample so as to monitor the microwave radiation output from the sample simultaneously with the output from the photomuliplier. Figure XX-7 illustrates the experimental arrangement.

A sample was constructed and mounted on the cold finger, and DC electric and
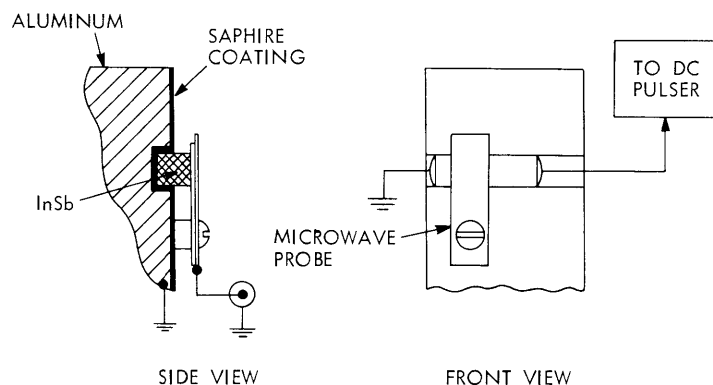
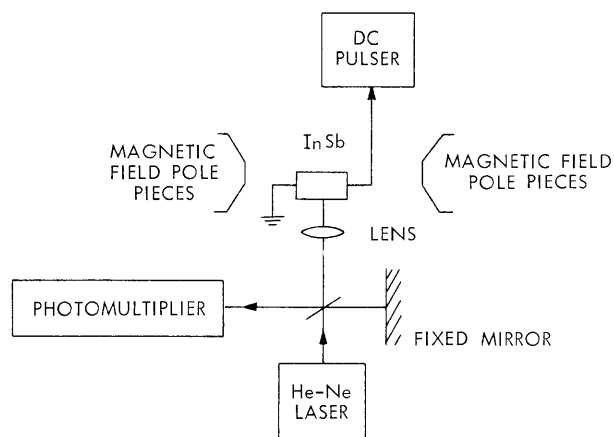Fig. XX-6. InSb sample holder attachment for a cold finger.

Fig. XX-7. Experimental arrangement.

magnetic fields were applied to the sample. A large amount of microwave noise was detected from this sample. The laser light was then focused to a small spot and moved so as to probe the surface of the sample from approximately its middle to one end. Optical probings were made for both polarities of DC electric field.

Preliminary results on this one sample indicate that the signal attributable to phonon activity is down into the noise of the receiver. This indicates that if there is surface motion at all, it is smaller than $\sim$(0.4) $\mathring{A}$. The He-Ne laser will create electron-hole pairs at the surface, and these could possibly alter locally the emission process. Work is under way to coat the surface with a very thin layer of insulation, and then apply a very thin gold overcoating so that the laser light will not penetrate to the surface of the InSb. We plan also to probe the end of the sample because if the phonons propagate exactly along the magnetic field, the technique of probing the surface of the sample would not detect them.

E. V. George, Marie D. Beaudry

References

1. C. Hartman, "Direct Coupling of an Acoustic Wave in a Piezoelectric Semiconductor to an Electromagnetic Wave in Free Space," S. M. Thesis, M. I. T., August 19, 1968.

2. MICROWAVE RADIATION FROM BiSb ALLOYS[*]

Introduction

Microwave radiation has been observed from electrically biased (as low as 0.9 V/cm) BiSb alloys at 4.2°K. The radiation is observed in the absence of a magnetic field and, moreover, is very sensitive even to weak magnetic fields. Radiation is observed from semiconducting BiSb alloys, but not from the semimetallic alloys. The purpose of this study was to examine BiSb alloys for microwave radiation.

Sample Information

The band structure of $Bi_{1-x}Sb_x$ alloys has been the subject of a number of investigations[1-4] in the small x region. While the details of the band structure are still being debated,[5] it is generally agreed[1,2] that for antimony concentrations of $x \leq 0.05$ to 0.07 the alloys are semimetallic, with overlapping conduction and valence bands. Above x = 0.05 to 0.07 the system becomes a semiconductor with a very small energy gap that increases with increasing (up to approximately x = 0.15) Sb concentrations. We have

---

examined some of these alloys (from x = 0.00 to 0.12) for emission of microwave radiation when the samples are cooled to cryogenic temperatures and subjected to biasing electrical and magnetic fields.

The samples were cut from boat-grown BiSb alloys prepared from 6-9 pure Bi and Sb. The crystals were grown by utilizing magnetic stirring and very slow growth rates in order to avoid constitutional supercooling. Examination of the resulting alloys with x-ray fluorescence showed that the alloys were uniform to better than 0.5%. The samples were cut either with a jeweler's saw or spark cutter to rectangular parallelepipeds having typical approximate dimensions of $1 \times 1 \times 10$ mm^3, and the surfaces were lapped and polished to an optical finish. The concentrations and mobilities of most samples were determined by conventional Hall or helicon techniques. Gold wires were soldered to the ends of the samples with a variety of solders with low melting points. The samples were then placed near the end of a coaxial transmission line immersed in a cryogenic fluid with a magnetic field parallel to the sample current direction. The transmission line was connected to a conventional radiometer with a sensitivity of ~10^{-14} W. The system had been previously used to investigate[6] microwave radiation from InSb. Microsecond current pulses were applied to the low-impedance samples by means of a strip line.

Microwave Emission Results

Table XX-3 lists the samples tested for microwave radiation (1-3 GHz), gives their concentration and mobility, and states whether or not radiation was observed from them. The most striking aspect of this table is that no microwave radiation (with various combinations of current densities to ~20,000 A/cm^2 and magnetic field to 5 kG) was observed

Table XX-3. Samples in which radiation was sought (T = 4.2°K).

Sample	Concentrations	Mobility	Radiation
Bi	$n = p = 2.5 \times 10^{17}/cm^3$	10^7 cm^2/V-sec	No
Bi$_{97}$Sb$_{03}$	$n = p = 4 \times 10^{16}/cm^3$	?	No
Bi$_{95}$Sb$_{05}$	$n = $?	?	No
Bi$_{95}$Sb$_{05}$	$n = 7.1 \times 10^{15}/cm^3$	160,000 cm^2/V-sec	Yes
Bi$_{92}$Sb$_{08}$	$n - 2.3 \times 10^{16}/cm^3$	2,000,000 cm^2/V-sec	Yes
Bi$_{88}$Sb$_{12}$	$n = 4.8 \times 10^{15}/cm^3$	220,000 cm^2/V-sec	Yes

from samples having ≤5% Sb concentrations, whereas radiation is observed from all samples having concentration in excess of this value. (The reason why one 5% alloy radiates and the other does not is unknown, unless they have small differences in concentration.) This strongly suggests that the semimetallic alloys do not radiate microwaves, whereas the semiconducting ones do.

The radiation as a function of electric field was typically a combination of spiked and continuum radiation; sometimes the spikes came at lower electric fields than the continuum and sometimes vice versa. The threshold characteristics for microwave emission from BiSb alloys were found to be vastly different from the threshold characteristics for InSb.[7] In BiSb alloys the effect of increasing magnetic field was first, to increase the electric field threshold from its minimum value at zero magnetic field, and second, to completely quench the radiation. In some of the alloys the magnetic field required to quench the radiation was 100-200 G. The effects of the externally applied magnetic field are complicated by the fact that the self-fields of the sample current were 10-40 G at the surface of the sample at the onset of radiation.

Figure XX-8 shows a series of curves of microwave radiation of 1 GHz from the 12% Sb sample taken at various values of magnetic field. As well as showing the effect of magnetic field on the structure, each of the curves has a series of spikes that come closer together as they approach the threshold for the background continuum radiation. For the 8% Sb sample there was no continuum radiation, but the radiation consisted of a series of discrete spikes. The spike structure of all samples, furthermore, was sensitive to the polarity of the electric field. Our sample resistances were very low (always < 0.5 Ω) and very nearly ohmic for both directions of current until impact ionization conditions[8] were reached. Each of the three samples giving rise to radiation employed a different solder with low melting point. The solders used in 5, 8, 12% Sb samples were Wood's metal, BiSnPb (Au doped), and In solders. Various of these same solders were also used in the nonradiating samples.

No radiation was observable from the bismuth-antimony alloys at liquid-nitrogen temperatures.

Microwave Emission (Spike) Spectra

To examine the frequency spectra of the spiked emission from BiSb alloys, the pulsed microwave output from the coaxial sample holder was fed directly into an RF spectrum analyzer. To reduce the ambiguity regarding image frequencies on the spectrum analyzer display, use was made of bandpass filters. The synchroscope (video) output of the spectrum analyzer was displayed on an oscilloscope simultaneously with the voltage across the sample. The dispersion of the spectrum analyzer was set to its minimum value (~1 MHz), in order to reduce the uncertainty in the measured frequency.
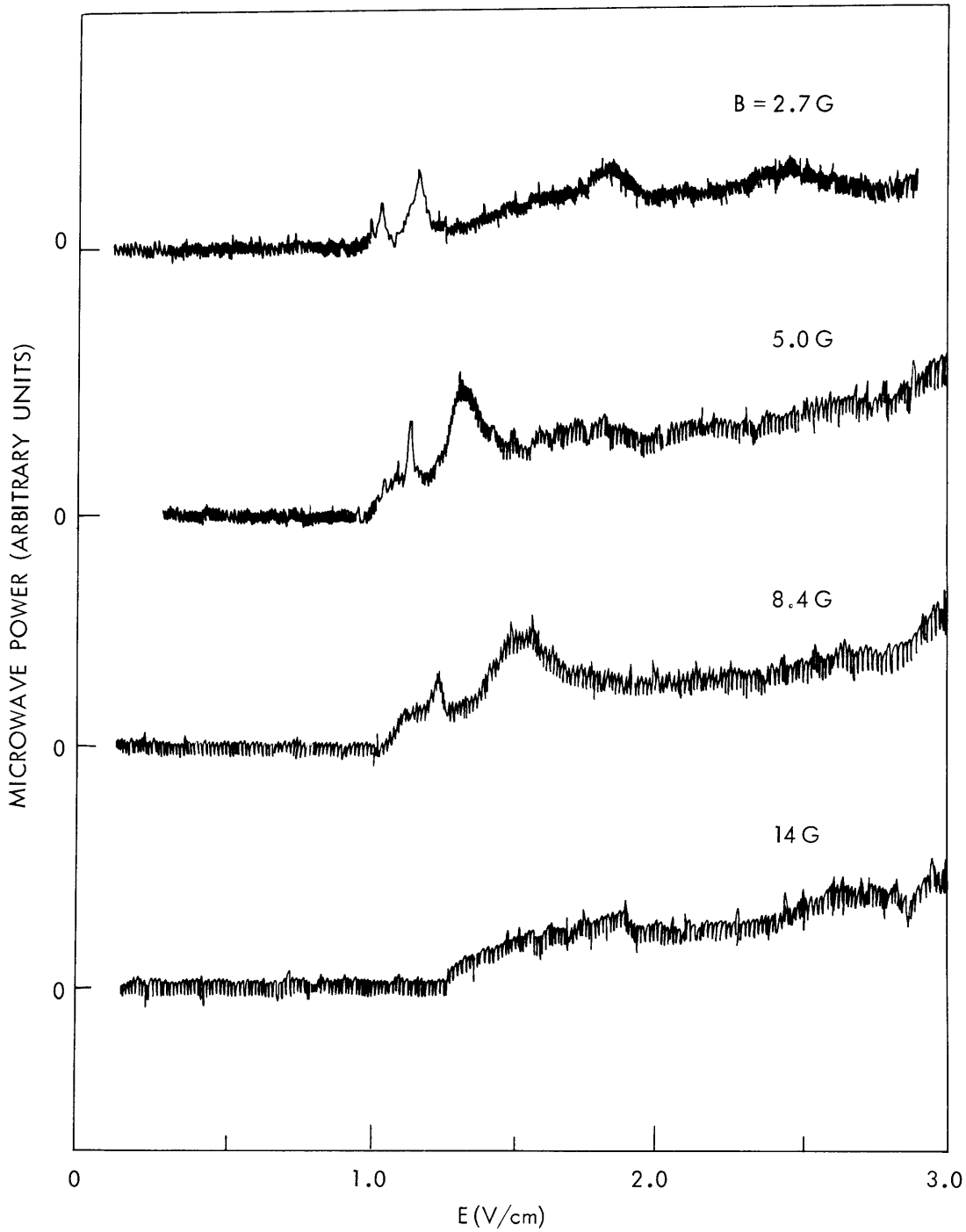
Fig. XX-8. Curves of 1-GHz (bandwidth, 10 MHz) microwave emission as a function of electric bias for several values of magnetic field in $Bi_{88}Sb_{12}$. Attenuation in the top curve is 6 dB, and 2 dB in others. T = 4.2°K.
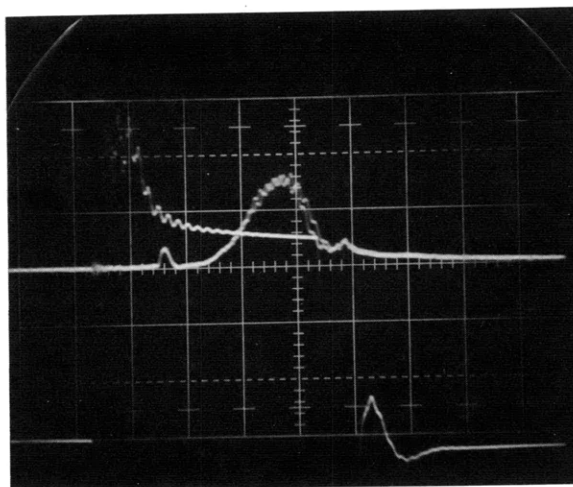
Fig. XX-9. Synchroscope (Video) output and voltage pulses applied to the sample as a function of time. Horizontal scale (time), 1 µsec/cm; vertical scales 5 V/cm (voltage), 0.5 V/cm (Video). Observation frequency, 2330 MHz.

Figure XX-9 illustrates both the voltage pulse and synchroscope output from the $Bi_{92}Sb_{08}$ sample. This sample was chosen, since its microwave emission consisted of spike emission with no continuum radiation.

Figures XX-10 and XX-11 illustrate the electric field frequency dependence for the spiked emission from $Bi_{92}Sb_{08}$ at constant magnetic field. Many interesting features are evident from these figures. For a given spike there is a minimum frequency below which the spike fails to appear; this minimum frequency was called the apex frequency. The output from the synchroscope was dramatically different when the spiked radiation was at the apex frequency. This is illustrated in Fig. XX-12. The positions of the apex frequencies in Figs. XX-10 and XX-11 are denoted by the symbol X. These frequencies (for the mid-electric field range) were f_1 = 775 MHz, f_2 = 1540 MHz, f_3 = 2320 MHz, and f_4 = 3110 MHz. This type of spectrum is suggestive either of nonlinear generation of higher harmonics or parametric coupling of two or more waves. It was also observed that the lower frequency spikes emitted more microwave power than the higher frequency spikes.

In taking the data for Fig. XX-10 a triggering problem in the voltage pulser caused the sample to be heated. This heating apparently caused some sample damage. Figure XX-11 gives data taken after sample damage. The effect of this damage appeared only to shift the electric field position of the spike apex but not its frequency.

To see whether heating was affecting the shape of the upper portion of the curves at higher sample voltages, the temperature of the liquid helium was lowered below its
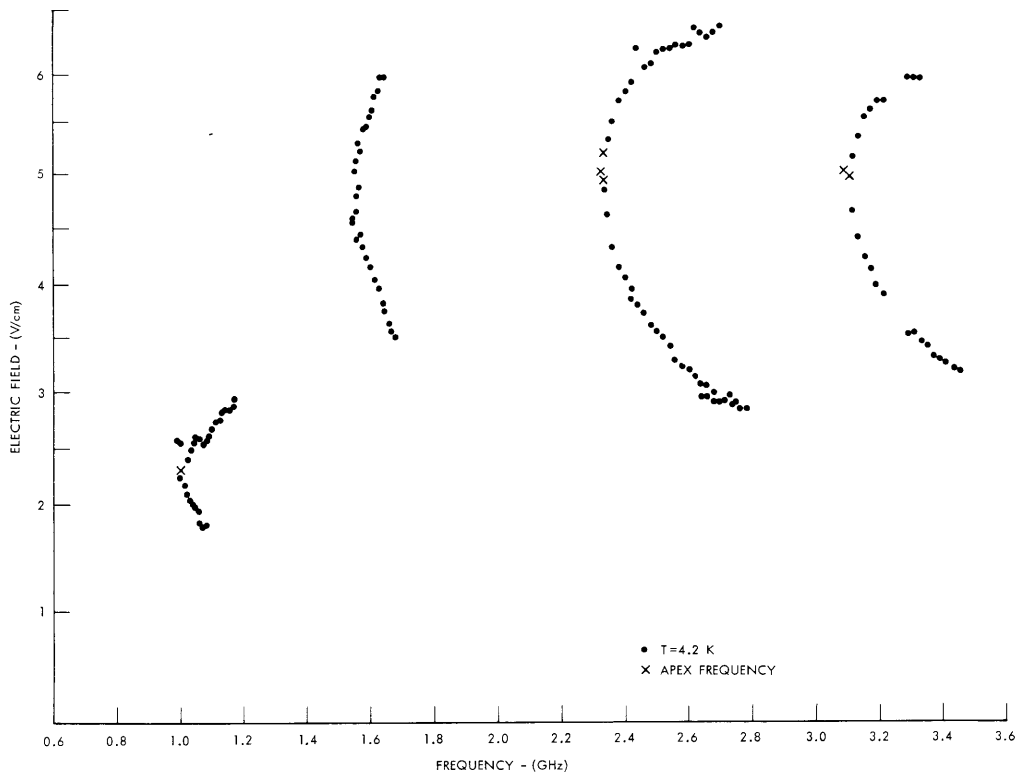
Fig. XX-10. Frequency, electric-field dependence of spiked emission from $Bi_{92}Sb_{08}$ at constant magnetic field of 2. 9 G. T = 4. 2°K before sample damage.
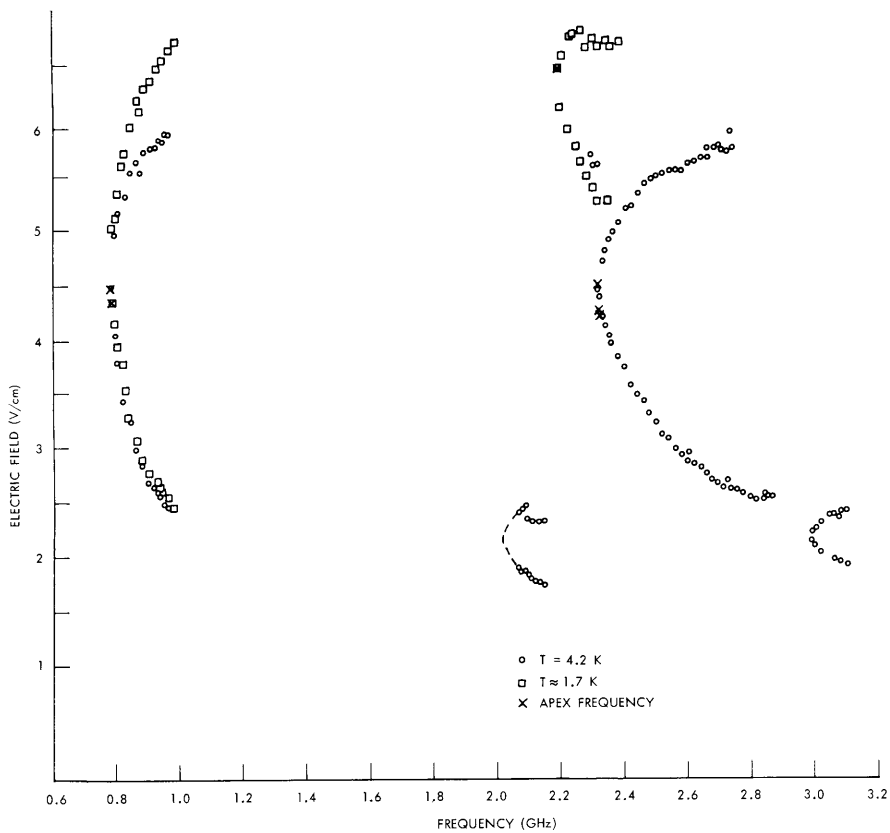

Fig. XX-11.

Frequency, electric-field dependence of spiked emission from $Bi_{92}Sb_{08}$ at constant magnetic field of 2. 8 G, for two sample temperatures, 4.2°K and 1.7°K, after sample damage.

Fig. XX-12.

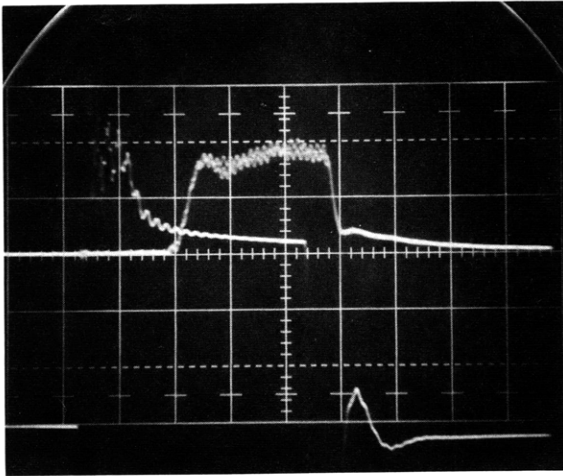Synchroscope (Video) output and voltage pulse applied to the sample as a function of time. Horizontal scale (time) 1 μsec/cm; vertical scales, 5 V/cm (voltage), 0.5 V/cm (Video). Observation frequency, 2320 MHz (Apex).
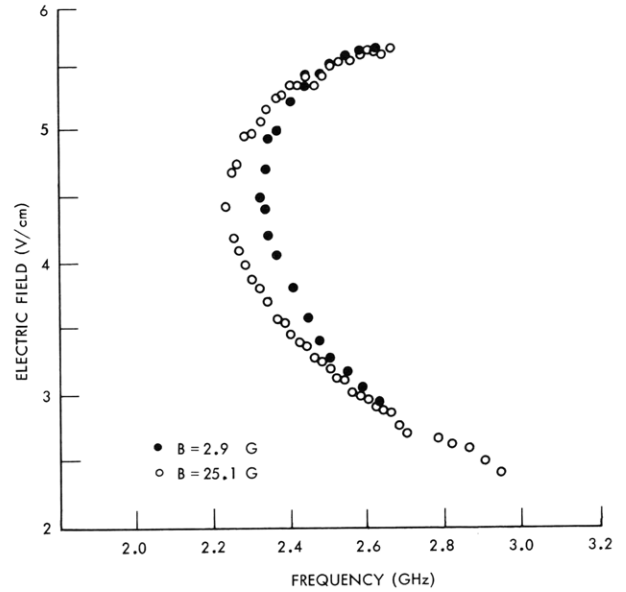

Fig. XX-13.

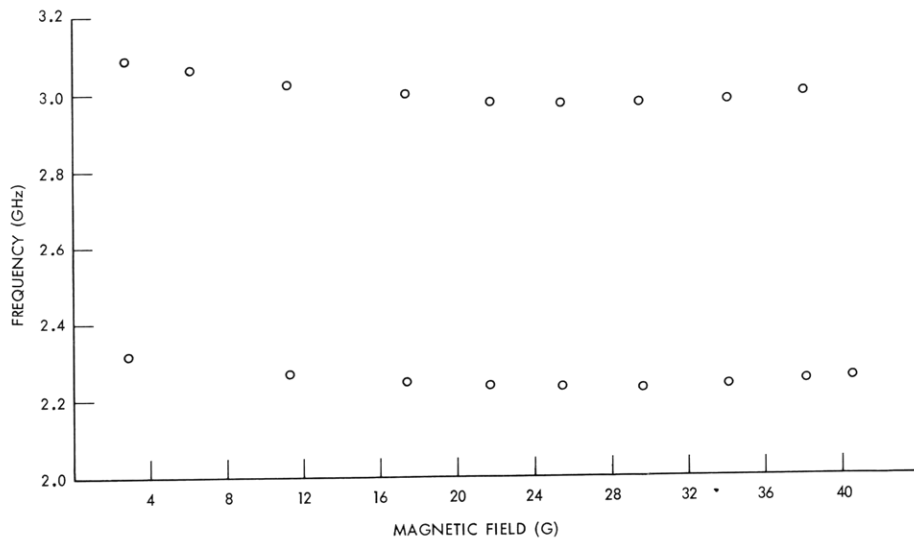Spike spectrum for two values of magnetic field for the $Bi_{92}Sb_{08}$ sample. T = 4.2°K.

Fig. XX-14. Apex frequency, magnetic-field characteristics for the $Bi_{92}Sb_{08}$ sample. T = 4.2°K.

λ-point. At this lower temperature the shape of the curve about an apex is more symmetric. The data taken at this lower temperature are illustrated in Fig. XX-11 and is denoted by the symbol □ . At this lower temperature we also found another spike branch at higher sample voltages. Notice also (Figs. XX-10 and XX-11) that the electric field at the apices occurs at approximate multiples of the lowest electric field apex.

In Fig. XX-13 the effect of magnetic field on the shape of a spike spectrum is illustrated, and in Fig. XX-14, the effect of the magnetic field on the frequency of two apices.

C. A. Nanney, E. V. George
[Dr. C. A. Nanney is at Bell Telephone Laboratories, Murray Hill, New Jersey.]

References

1. A. L. Jain, Phys. Rev. 144, 1518 (1959).

2. S. Tanuma, J. Phys. Soc. Japan 14, (1959).

3. S. Mase, J. Phys. Soc. Japan 13, 434 (1958); 14, 585 (1959).

4. D. M. Brown and S. J. Silverman, Phys. Rev. 136, 290 (1964).

5. S. Golin (to appear in The Physical Review).

6. E. V. George, Quarterly Progress Report No. 88, Research Laboratory of Electronics, M.I.T., January 15, 1968, pp. 202-204.

7. E. V. George, Quarterly Progress Report No. 90, Research Laboratory of Electronics, M.I.T., July 15, 1968, pp. 108-111.

8. C. A. Nanney (submitted for publication).

XX. APPLIED PLASMA RESEARCH[*]

C. Plasma Physics and Engineering

Academic and Research Staff

Prof. D. J. Rose	Prof. E. P. Gyftopoulos	Prof. T. P. Ziebold
Prof. T. H. Dupree	Prof. L. M. Lidsky	Dr. R. A. Blanken
	Prof. W. M. Manheimer	

Graduate Students

N. M. Ceglio	M. Hudis	K. Ohmae
H. Ching	T. R. Hulick	C. E. Wagner
D. G. Colombant	M. A. LeComte	R. J. Vale
	G. R. Odette	

RESEARCH OBJECTIVES AND SUMMARY OF RESEARCH

1. High-Intensity 14-MeV Neutron Source

Our investigation of a possible design for a 14-MeV neutron source with 10^{15} n/sec total intensity is being continued. The source is small enough to achieve a surface flux of 10^{14} n/cm^2 sec at this intensity — a flux high enough to test materials for fusion reactor use. The key feature of the source is the use of the Mach line of a freely expanding gas jet as the target for a high-energy tritium beam. The gasdynamic problem has been solved; we are proceeding to study the optimum system parameters and scaling laws.

D. C. Colombant, L. M. Lidsky

2. Stuffed Cusp Experiment

Our original objective in this work was the investigation of the stability boundaries of hot-electron plasmas in several magnetic field structures. The plasma, formed by the beam-plasma interaction, has turned out to be very complex. We have therefore turned to a simpler version of the original problem — an attempt to measure and understand the nature and stability boundaries of the observed electron-cyclotron frequency instabilities. We shall use the plasma data gathered in pursuit of our first objective in conjunction with measurements obtained by use of a new high-frequency probe in this effort.

C. E. Wagner, L. M. Lidsky

3. Smaller Scale Experiments

We shall continue some smaller scale experiments based on the use of the HCD plasma source. These experiments are generally done as Master's research topics of approximately one year duration. The topics are chosen for their combination of educational merit and scientific interest. Present topics include plasma rotation studies by Doppler-shift interferometry, diffusion studies by tracer injection, and ion acoustic wave propagation in the low-frequency ($\omega < \omega_{ci}$) regime.

L. M. Lidsky

4. Pulsed 10.6 μ Laser Systems

We are investigating several schemes for increasing the Q-switch power output of the 10.6 μ H_2-CO_2-He laser systems. The most promising idea at the moment involves using the afterglow of a high-pressure strongly excited discharge. The objective of this study, in addition to our increased understanding of the dynamics of the N_2-CO_2-He excitation transfer processes, is the development of simple techniques capable of producing pulses in the 0.1-1.0 MW peak power range.

L. M. Lidsky

5. Plasma Transport in the Hollow-Cathode Discharge

Although it is generally agreed that fluctuating electric fields are the cause of experimentally observed enhanced plasma transport, the expected quantitative relations between the magnitude and frequency of the fluctuations and the speed and direction of transport are not often satisfied. We have developed a new technique for the direct measurement of diffusion flux and are using it to investigate plasma flows in the HCD. Our immediate goals are twofold.

a. To understand and control the coherent and turbulent oscillations of the plasma column. This will allow us to observe the nature of plasma transport in regimes in which directed drifts are dominant and in which true stochastic diffusion is dominant.

b. To compare the measurements obtained with our new synchronous probe technique with those obtained by density-potential correlation techniques under the same conditions. This will aid us in understanding why correlation techniques often fail.

M. Hudis, L. M. Lidsky

6. Plasma Confinement in a Levitron of Small Aspect Ratio

Construction of a model Levitron of small aspect ratio with a supported 10-cm diameter ring has been completed. Plasma is produced via electron-cyclotron resonance heating at 2.8 GHz with up to 1 MW of power being supplied in a 10-μsec pulse. We plan to study plasma confinement in this device, focusing particular attention on the relationship between the structure of the low-frequency electric fields and diffusion.

R. A. Blanken, A. S. Ratner

7. Synchrotron Radiation from High-Density Plasmas

During this past year, the synchrotron emission from hot test electrons immersed in a dense background plasma has been examined theoretically and compared with previously obtained experimental data. Using the results of these studies, we plan to examine the synchrotron radiation process in high-density plasmas, especially in relation to the energy balance of mirror reactors.

R. A. Blanken

8.

The nonlinear stabilization of a variety of linearly unstable waves that propagate at multiples of the electron or ion cyclotron frequencies is being studied theoretically. Many of these waves become damped if real ω is shifted by a small amount $\Delta\omega \ll \omega$. Such waves are easily stabilized if nonlinear effects broaden the wave-particle resonance by an amount $\Delta\omega$.

T. H. Dupree

9. A fine scale granulation of the plasma density is caused by the semirandom convection of plasma by waves. This granulation appears to produce some interesting effects that are being investigated theoretically. For example, the grains or blobs can produce greatly enhanced Bremsstrahlung cyclotron radiation. The granulation also leads to a greatly enhanced fluctuation spectrum over a wide range of frequency and wave number. Such spectra are observed experimentally but do not seem to be just a superposition of plasma waves.

T. H. Dupree

10. The nonlinear properties of a standing drift wave are being studied by following ion trajectories numerically on a digital computer. In this way, one can obtain the harmonic distortion in the wave, particle transport across the field, and other quantities that can be compared with experiments.

H. Ching, T. H. Dupree